Power Network Reliability Framework for Integrating Cable Design and Ageing

Konstantinos Kopsidas, *Senior Member, IEEE*, and Shuran Liu, *Student Member, IEEE*

***Abstract*—Utilities are challenged to develop economically competitive plans for expanding power transfer capabilities and increasing network resilience under uncertainties. To overcome these challenges, utilities frequently operate their underground cable systems with flexible ratings under planned or emergency network contingencies. At present, the increased risk associated with such an emergency loading operation of cables and networks is not quantified. To address this gap, the paper presents a novel advancement in existing methodology for evaluating power network reliability, which accounts for the increased risk of failures and ageing that underground cables experience during emergencies. The proposed framework integrates a double sequential Monte Carlo simulation loop with a detailed cable system model incorporating important plant design properties. This integration captures the risk of cable ageing at emergency events within a multiyear network analysis. The methodology is demonstrated on the modified IEEE 14-bus network with long- and short-term emergency ratings under both steady-state and transient electro-thermal implementations. Crucially, the methodology can inform utilities about the emergency loading risks for network performance, including adequacy, resiliency, flexibility, and cable ageing.**

***Index Terms*—Ageing, asset management, emergency ratings, flexibility, power cables, power system planning, probabilistic methods, reliability assessment, resilience, thermal inertia.**

NOMENCLATURE

The symbols used throughout this paper are defined below.

A. Indices

i	Cable number running from 1 to c
i'	Normal-loaded cable, $\forall\, i' \in c$
i''	High-loading cable, $\forall\, i'' \in c$
j	Network bus number running from 1 to $j_{\max}$
k	Layer number for cable and soil running from -m to n
x	Network load point number running from 1 to N_D
y	Network generator number running from 1 to N_g
Y	Simulation year running from 1 to N
Y_L	Simulation life-cycle year running from 1 to Y_{Life}

B. Parameters

Design risk coefficient

β	Ageing acceptability risk coefficient
β_{i,Y_L}	Ageing acceptability risk coefficient of cable i at Y_L
Δt	Time-step of SMC annual computation, $\forall \Delta t \in Y$
$\theta_{\mathrm{a}}(t_{\Delta t})$	Ambient soil temperature at $t_{\Delta t}$
$\theta_{Ar,i}(t_\theta)$	Armour temperature of cable i at t_θ
$\theta_{C,i}(t_{\Delta t})$	Expected cable conductor temperature of cable i at $t_{\Delta t}$
$\theta_{C,i}(t_\theta)$	Expected cable conductor temperature of cable i at t_θ
$\theta_{o,i}$	Ambient soil reference temperature of cable i
$\theta_{S,i}(t_\theta)$	Screen temperature of cable i at t_θ
$\theta_{\mathrm{SL}(k)}$	Soil temperature at the layer $k\,(1 \le k \le n)$
$\lambda_{N,i'}$	Failure rate of normal loaded cable i'
$\lambda_{E,i''}$	Failure rate of emergency loaded cable i''
$\lambda_{LTE,i''}$	Failure rate of long-term emergency loaded cable i''
$\lambda_{STE,i''}$	Failure rate of short-term emergency loaded cable i''
$\mu_{N,i'}$	Repair rate of normal loaded cable i'
c	Total number of cables in the network
$C_{C,i}$	Conductor thermal capacitance of cable i
$C_{d,i}$	Insulation thermal capacitance of cable i
$C_{S,i}$	Screen thermal capacitance of cable i
$C_{Ar,i}$	Armour thermal capacitance of cable i
$C_{J,i}$	Jacket thermal capacitance of cable i
$C_{\mathrm{SL}(k)}$	Thermal capacitance of soil layer k ($1 \le k \le n$)
D^x_{actual}	Actual supplied load at load point x
D^x_{total}	Total load required at load point x
Ea_i	The material's activation energy of cable i
G_y	Generation output capability of generator y
$I_{i,flow}(t_{\Delta t})$	Current flow of cable i at time $t_{\Delta t}$
$I_{con,i}$	Maximum normal continuous current of cable i
$I_{LTE,i}$	Long-term emergency loading current of cable i. $I_{STE,i}$ Short-term emergency loading current of cable i
k_B	The Boltzmann's constant (in eV/K)
ℓ_i	Total length of cable i
$L_{o,i}$	Expected life of cable i when it operates at $\theta_{o,i}$
$LF_{\theta_{C,i}}(t_{\Delta t})$	Loss-of-life fraction within Δt of cable i at θ_C
m	Total number of cable conductive component layers
n	Total number of soil layers
N	Maximum number of repetitions of annual simulations within the 1st SMC-loop

Manuscript received October 11, 2016; revised March 5, 2017 and June 1, 2017; accepted June 11, 2017. Date of publication August 9, 2017; date of current version February 16, 2018. This work was supported in part by the EPSRC HubNet EP/N030028/1. Paper no. TPWRS-01525-2016. *(Corresponding author: Konstantinos Kopsidas.)*

The authors are with the School of Electrical and Electronic Engineering, University of Manchester, Manchester M13 9PL, U.K. (e-mail: k.kopsidas@manchester.ac.uk; shuran.liu@postgrad.manchester.ac.uk).

Color versions of one or more of the figures in this paper are available online at http://ieeexplore.ieee.org.

Digital Object Identifier 10.1109/TPWRS.2017.2720196

N_D	Number of load points in the network
N_g	Number of generators in the network
$\mathrm{P_{T\text{-}a}}$	External thermal power induced in ambient
$\mathrm{P_{T\text{-}Ar}}$	External thermal power induced in cable's armour
$\mathrm{P_{T\text{-}C}}$	External thermal power induced in cable's core
$\mathrm{P_{T\text{-}}}k$	External thermal power induced in layer k of the thermo-electric-equivalent cable model
$\mathrm{P_{T\text{-}S}}$	External thermal power induced in cable's sheath
$p_g^{\,y}$	Real generated power by generator y
$q_g^{\,y}$	Reactive generated power by generator y
S_i	Power flow within cable i
$S_{\max,i}$	Maximum power flow of cable i
SS-$\theta_{C,i}(t_\theta)$	Steady-state conductor temperature of cable i at t_θ
TS-$\theta_{C,i}(t_\theta)$	Transient-state conductor temperature of cable i at t_θ
$t_{\Delta t}$	Time vector for time-step analysis (1st SMC-loop)
t_θ	Time vector for cable thermal modelling
$T_{Arm,i}$	Thermal resistance of the armour of cable i
$T_{Ins,i}$	Thermal resistance of the insulation of cable i
$T_{J,i}$	Thermal resistance of the jacket of cable i
$T_{\mathrm{SL}(k)}$	Thermal resistance of soil layer k ($1 \leq k \leq n$)
$T'_{(k)}$	Thermal resistance of layer k in TEE model
$TTF_{N,i'}$	Time-to-fail of normal loaded cable i'
$TTF_{LTE,i''}$	Time-to-fail of long-term emergency loaded cable i''
$TTF_{STE,i''}$	Time-to-fail of short-term emergency loaded cable i''
$TTR_{N,i'}$	Time-to-repair of normal loaded cable i'
$TTR_{E,i''}$	Time-to-repair of emergency loaded cable i''
U_{i,Y_L}	Unavailability of cable i at year Y_L
$U_{N,i'}$	Unavailability of normal loaded cable i'
$U_{LTE,i''}$	Unavailability of long-term emergency loaded cable i''
$U_{STE,i''}$	Unavailability of short-term emergency loaded cable i''
V_j	Voltage of network bus j
$W_{C,i}(t_{\Delta t})$	Conductor losses of cable i at time $t_{\Delta t}$
$W_{S,i}(t_{\Delta t})$	Screen losses of cable i at time $t_{\Delta t}$
$W_{Ar,i}(t_{\Delta t})$	Armour losses of cable i at time $t_{\Delta t}$
Y_{Life}	Maximum number of life years for network life-cycle analysis (2nd SMC-loop)

C. Functions

$f_D^{\,x}(\cdot)$	Damage cost function for curtailed demand at point x
$f_P^{\,y}(\cdot)$	Real power generation cost function at point y
$f_Q^{\,y}(\cdot)$	Reactive power generation cost functions at point y

I. Introduction and Background

POWER networks currently encounter a multifaceted challenge involving sustainability, security, competition and reliability. In particular, they are expected to: (a) accommodate the continuously increasing electricity demand, (b) efficiently expand to provide connection to remote renewable energy sources, (c) be more resilient and reliable under uncertainties, and (d) be optimally utilized. To overcome these challenges, utilities deploy alternative economic and flexible methods to increase network power flow capacities instead of building new infrastructure. One implementation is probabilistic thermal rating which involves an additional risk, when compared to static thermal rating, due to the larger probabilities used for exceeding the operating temperature [1]–[3]. Another option is real-time monitoring instrumentation for time-varying (e.g., seasonal, hourly) line ratings [4]–[6]. Other ways to increase adequacy exploit flexible operating practices that allow emergency ratings at critical loading events [7]–[9].

Although flexible network-expansion increases power transfer economically, such solutions relax the thermal constraints and thus carry the additional risk of thermal ageing that is not captured within existing network evaluation modelling methods.

Underground cable (UGC) systems have large thermal inertia due to the mass of conductive, insulating and surrounding (soil) materials [10]. Thus, there is a significant time delay between an increase in cable current flow and the corresponding cable temperature increase [11]. This time delay provides utilities with the capability to load their cables at higher current ratings, sometimes up to twice the normal rating, for short durations under emergency conditions [10]. For example, IEEE standards determine the admissible emergency overload capacity of XLPE cables at 130 °C for 36 hours [12]. Data for long-term emergency (LTE) and short-term emergency (STE) ratings after a contingency event are also provided in [13]. Even though UGC emergency ratings are known to utilities and frequently applied [14]–[16], most of the existing studies only evaluate the benefits from increased adequacy provided by hourly-varying thermal ratings [17], [18]. The literature that integrates the benefits and risks of emergency rating operation on a network-wide analysis is still limited.

Two basic elements should be considered in the development of realistic and practical models for UGC emergency ratings: (a) a thermal-rating model that considers UGC design properties and (b) a thermal-ageing model that considers the 'overheating' effects on the cable and consequently the intrinsic risks of cable degradation. Many UGC thermal-rating models are developed based on finite element analyses [19], [20] and thermo-electric equivalent circuits [10], [21] to calculate a cable's conductor temperature for given current flow and design properties. Such models have been implemented within network-wide studies [22]. Yet, these studies do not consider the cable's thermal inertia, which is a dominant factor for increasing the network's flexibility but most critically they do not consider the anticipated thermal ageing of the cable.

Although there are studies on plant design that quantify the impact of the thermal ageing on cable lifetime estimation [11], [23], there is limited work that considers cable ageing into network reliability evaluations [24]–[26]. Furthermore, previous studies fail to capture the thermo-electrical and thermo-mechanical effects on cable ageing due to emergency loading conditions, which actually dominate the ageing of the plant and result in increased risk of failure [11], [27].

This paper proposes advancements in the reliability assessment methodology to capture the increased network flexibility and ageing risks associated with the implementation of emergency loadings on cables. This risk–flexibility worth

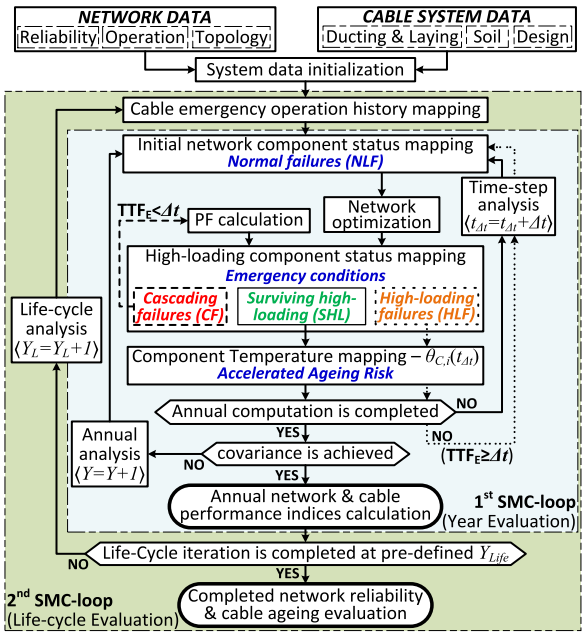

Fig. 1. The computation framework of the double SMC, including the life-cycle evaluation, and the additional high-loading operating status mapping of cables

methodological addition is executed through the inclusion of *three new high-loading* operating states on cable modelling, and *a life-cycle simulation loop* on network modelling. The combination of these high-loading component states and the life-cycle loop allows capturing the benefits from increased network flexibility when utilizing emergency ratings but also the penalties associated with ageing risk and increased failure risk of cables with extensive emergency loading history.

Section II describes the integration of UGC system electro-thermal design properties within the network-wide reliability framework. Section III presents the implementation of the methodology with an example case study, and Section IV discusses the key findings and outputs of the case study. Finally, Section V concludes with the impact of the methodology and the issues that worth further development.

II. Reliability Evaluation Framework Integrating UGC Electro-Thermal Design and Ageing

A. Outline of the Computations

To capture the risk of cable failures due to emergency loading operation, the proposed methodology integrates a combined detailed thermal and ageing modelling of UGCs within a network reliability analysis. This integration is achieved through the implementation of a double sequential Monte Carlo (DSMC) simulation loop illustrated in Fig. 1. The 1st SMC-loop calculates the annual reliability for every network cable while the 2nd SMC-loop performs network analysis considering the cables' life-cycle degradation in annual steps. Using this approach, the network performance can be evaluated while considering the effect of cables' emergency loading thermal ageing for long-term operation and planning assessments.

The input *network data* block defines the failure/repair rates of network components, the voltage and thermal (emergency/normal) operating constraints, the operating limits of generating units and cost functions, the load points and their chronological demand, the network layout and spatial arrangement, as well as the component impedances and their designed voltage levels. The *cable system data* define the design properties of the plant, including cable properties, laying configuration, surrounding environment and real-time soil measurements.

The 1st SMC-loop implements two distinct cable operation status mappings for *normal failures* and *emergency conditions* indicated in Fig. 1 as *Initial network component status mapping* and *high-loading component status mapping,* respectively. This approach helps to calculate the increased probability of component failures and ageing, expected at emergency loading. It performs analyses for a single year, $Y, \forall Y \in \{1, \cdot, N\}$ in a sequential time vector, $t_{\Delta t}$, segmented in steps, Δt, $\forall \Delta t \in Y$ [28].

This 1st SMC-loop initially captures all the *Normal failures* prior to investigating any consequent *Cascading failures* (CF) and *High-loading failures* (HLF), due to the emergency loading operation, which might occur after the *Network optimization* is performed to address any constraints due to normal failures. In Fig. 1 it can be seen that the cascading failures do not feed into the network optimization considering the real scenario of operators' inability to perform a corrective action, due to an immediate thermal protection response. On the contrary, the high-loading failures do not occur instantly (in the same Δt) and therefore emergency loading provides operators with the additional flexibility to respond to initial *normal failures* by allowing higher post-fault loading of the components. Furthermore, there are high-loading events that do not necessarily lead to failures, i.e., *Surviving high-loading* (SHL). However, there is an increased risk associated with high-loading operation at emergency conditions, which justifies their limited use by the operators, only during network constraints. This is captured within the 1st SMC-loop by implementing the additional *component temperature mapping* block in Fig. 1, of every cable, *i*, to compute the expected cable temperature at every Δt, $\theta_{C,i}(t_{\Delta t})$ and the associated ageing risk. The thermal and ageing modelling implemented in this block is detailed in Section II-D, while the increased risk of failure expected on the high-loading components is captured via the dashed and dotted paths (in Fig. 1) and the emergency time-to-fail ($\mathrm{TTF_E}$) calculations (and transition paths) detailed in Section II-B2. The 1st SMC-loop is terminated based on the EENS covariance (cov) or after simulating a maximum set of years, *N* [29].

The 2nd SMC-loop calculates the cumulative effect of emergency loadings on cable insulation degradation and its impact on cable's life expectancy and failures. It is a life-cycle analysis performed in year-steps $Y_L, \forall Y_L \in \{1, \cdots, Y_{Life}\}$. This 'life-cycle' modelling loop aggregates the *annual network & cable performance indices* calcuated in the 1st SMC-loop (Fig. 1) of the previous network operation years (Y_L) in order to compute the updated probability failures of the aged cables. These probabilities are then used to compute the *cable emergency operation history mapping* block (Fig. 1) and initiate the calculations for the next sequential Y_L operating year. Thus, the

outputs of the *N*-year analysis of the 1st SMC-loop are used in the 2nd SMC-loop to update the network cables' emergency operation history mapping, and hence, include any past emergency operation and associated ageing risk, before re-initiating the 1st loop. This DSMC process is terminated once the final year, Y_{Life}, of the life-cycle analysis is simulated.

The outputs of the 1st SMC-loop evaluate the annual performance and are clustered into:

a) *Network performance indices*: the expected energy not served (EENS), expected frequency of load curtailment (EFLC), expected duration of load curtailment (EDLC), expected frequency of network failures (EFNF), expected equivalent network ageing (EENA), and expected interruption costs (EIC) [30], [8];

b) *Cable performance indices*: the expected equivalent cable ageing (EECA), the expected frequency of emergency loading (EFEL), the expected duration of emergency loading (EDEL), and the expected frequency of cable failure (EFCF).

The mathematical formulations of these indices are detailed in Section II-E. The 2nd SMC-loop calculates, sequentially, the cumulative values of the 1st SMC-loop indices for the complete life-cycle (Y_{Life}) analysis. Hence, the indices for any future (non-simulated) Y_L year have null values.

B. 1st SMC-Loop Component Status Mapping Computations

The component status mapping in the 1st SMC-loop captures the operating states of the network cables at any Δt. It is performed within two distinct but interlinked sequential computational steps for the normal loading failures (NLF) and emergency conditions (Fig. 1), described in the following sections. It should be noted that when a cable *i* is loaded at its normal range is annotated as *i'* while the same cable *i* becomes *"i"* when it is high-loaded (above $I_{con,i}$) at any Δt.

1) Initial Network Component Status Mapping—Normal Failures: This step calculates, for the complete simulation year under normal component loading, the initial transition times of every cable *i*, $\forall\ i \in c$, where *c* is the total number of cables in the network. An SMC simulation is applied, at the start of the 1st loop, using the commonly employed two-state Markov chain (Fig. 2, left). (1) and (2) determine the (annual initial) transition times between *normal-loading state* and *normal-failure state* of every normal-loaded cable i', $\forall i' \in c$. The normal failure, $\lambda_{N,i'}$, and repair, $\mu_{N,i'}$, rates are used to calculate the time-to-fail, $TTF_{N,i'}$, and time-to-repair, $TTR_{N,i'}$, values, with an unavailability, $U_{N,i'}$, randomly generated from a uniform distribution U(0,1) [29].

$$TTF_{N,i'} = -(1/\lambda_{N,i'}) \ln U_{N,i'} \tag{1}$$

$$TTR_{N,i'} = -(1/\mu_{N,i'}) \ln U_{N,i'} \tag{2}$$

2) High-Loading Component Status Mapping—Emergency Conditions: Once the transitions for all normal-loaded cables i' and year *Y* are identified, then the transitions of high-loading cables i'', $\forall i'' \in c$ such that $i' + i'' = c$, are detected, at every Δt. Thus the high-loading component status mapping is performed at Δt when emergency conditions exist, by using the three proposed high-loading operation Markov states (cascading failure, high-loading failure, and surviving high-loading) shown in Fig. 2. This transition mapping requires the network's current flows on all cables at every Δt, $I_{i,flow}(t_{\Delta t})$. These are computed using a network optimal power flow calculation at Δt, as summarized in Section II-F.

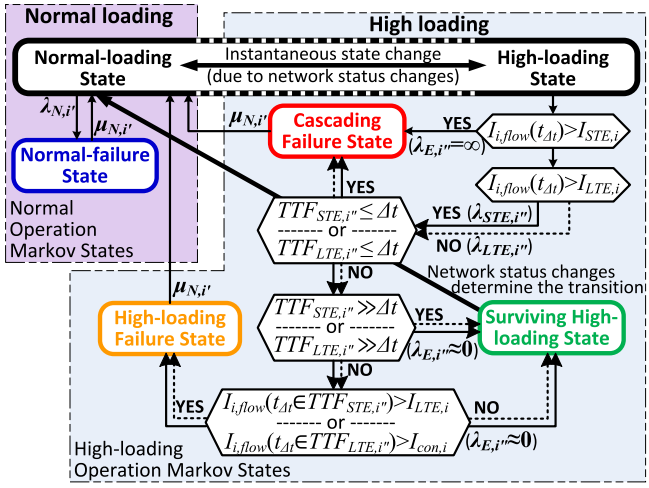

Fig. 2. Operation states and transition path probabilities of a cable *i* combining both its normal (i') and high-loading (i'') conditions. The double paths show the transitions that apply for either LTE (dashed) or STE (continuous) operation.

a) Transition path probabilities:: The component's transitions between normal-loading and high-loading states are instantaneous due to their network status dependency; i.e., are controlled by the network loading and the operating state changes of all other components (e.g., failures). Thus, these two states (for every *i*) are modelled as a single virtual state, as shown in Fig. 2, without any transition probability.

Every cable with a flow exceeding its maximum normal continuous current, $I_{con,i}$, is considered to operate at *high-loading state* and therefore, has an emergency time-to-fail (TTF_E) calculated using (3)–(8) for its short-term emergency (STE) and long-term emergency (LTE) design loadings.

$$TTF_{LTE,i''} = -(1/\lambda_{LTE,i''}) \ln U_{LTE,i''} \tag{3}$$

$$TTF_{STE,i''} = -(1/\lambda_{STE,i''}) \ln U_{STE,i''} \tag{4}$$

$$\lambda_{STE,i''} = \lambda_{N,i''} \times e^{((I_{STE,i}/I_{con,i})-1)\alpha} \tag{5}$$

$$\lambda_{LTE,i''} = \lambda_{N,i''} \times e^{((I_{LTE,i}/I_{con,i})-1)\alpha} \tag{6}$$

$$U_{STE,i''} = 1 - U_{N,i''}(I_{con,i}/I_{STE,i})^{\beta} \tag{7}$$

$$U_{LTE,i''} = 1 - U_{N,i''}(I_{con,i}/I_{LTE,i})^{\beta} \tag{8}$$

The unavailabilities $U_{STE,i''}$ and $U_{LTE,i''}$ are produced by (7) and (8) using two distinct random generators to facilitate the independence of the emergency loading events. These are functions of component loading since a higher risk of unavailability is involved with a higher (above normal) loading operation. Two new coefficients, α and β, are proposed to capture the design and operation risk aspects of the cable.

A design risk coefficient α, which is practically related to health indices of a component, is introduced here to define the risk of cable failure due to its design and condition. It takes into account the cable's design characteristics (e.g., laying in dry soil, under roads with a high complexity of repair works) as well as the level of repair and maintenance performed (e.g., no joints, no high voltage stresses, switching events, partial discharges, and other health indices utilities might implement). Thus, α, which has positive values, is set by the operator for each cable based on past experience and cable location awareness. A value $\alpha = 0$ indicates that a cable has null unfavorable conditions, very accessible to repair and recorded high health indices signifying a good maintenance.

An ageing acceptability risk coefficient β, which practically defines the risk-averseness of utilities on 'burning an asset', is introduced to determine the operator's willingness to utilize emergency loadings and to accept the corresponding cable ageing risk. It indicates the cable's previous emergency operation history and criticality on the network topology (i.e., other cables could adequately compensate its failure). β has also positive values with $\beta = 0$ indicating a new cable that has not experienced any emergency operation and whose load can be entirely diverted over other neighboring cables without any significant interruptions.

The repair time (TTR) calculation of high-loading events is set to be the same as that of the normal-loading events since it is difficult to predict the impact of the emergency failures on the component. Thus, the $TTR_{N,i'}$ and $TTR_{E,i''}$ are produced with a single $\mu_{N,i'}$ value for NLF, HLF, and CF of each cable *i* using (2)

b) High-loading states:: The ***cascading failure state*** describes the high-loading operation of a cable i'' leading to its failure within the same Δt. Three distinct transition paths can lead to a cascading failure as shown in Fig. 2. One path models the instant 'tripping' cable thermal protection, when $I_{i,flow}(t_{\Delta t})$ exceeds its designed STE loading, $I_{STE,i}$. Hence, for $I_{i,flow}(t_{\Delta t}) > I_{STE,i}$ the cable transition to cascading failure state is certain $(\lambda_{E,i''} = \infty)$. The other two paths that transition from high-loading to cascading failure, presented with the double arrow in Fig. 2, model the sudden failure (i.e., $\text{TTF}_\text{E} < \Delta t$) that occurs when the cable *i* is high-loaded (i.e., above $I_{con,i}$). One path of this double arrow (continuous line) captures the immediate failure probability of the cable when it operates within its STE loading (i.e., $I_{LTE,i} < I_{i,flow}(t_{\Delta t}) \leq I_{STE,i}$), which is described by the $TTF_{STE,i''} \leq \Delta t$, and it is calculated by (3). The other path (dashed line), in a similar manner, captures the failure probability of $TTF_{LTE,i''} \leq \Delta t$ for the cable operation within its LTE loading (i.e., $I_{con,i} < I_{i,flow}(t_{\Delta t}) \leq I_{LTE,i}$).

The ***high-loading failure state*** represents a failure due to the emergency loading of a cable i'' with a TTF_E that is larger than Δt. This failure affects the component's future states (i.e., at $t + \Delta t$ and beyond); thus the initial network component status mapping in Fig. 1 is updated to allocate these future state transitions. This is necessary as a normal failure will not occur if an emergency failure happened at the same time. The high-loading failures occur only when the high-loaded cables

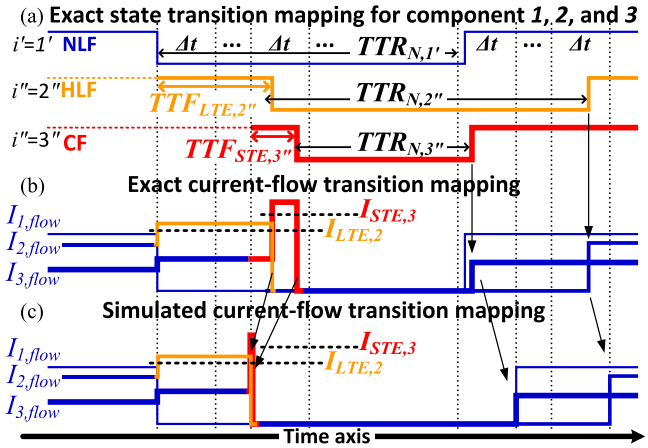

Fig. 3. An example of modelling the operating state transition times and their corresponding current flows.

i'' maintain their high-loading state for the complete estimated $TTF_{STE,i''}$ or $TTF_{LTE,i''}$ periods, as noted in Fig. 2. Consequently, the high-loading failures at STE (or LTE) loading occur when the following three conditions are satisfied: (a) the $TTF_{STE,i''}$ (or $TTF_{LTE,i''}$) is greater than Δt, (b) the $TTF_{STE,i''}$ (or $TTF_{LTE,i''}$) are relatively small (i.e., less than 36 hours), and (c) the current flow of the cable is continuously maintained at the STE (or LTE) level during the entire $TTF_{STE,i''}$ (or $TTF_{LTE,i''}$); so it should be $I_{i,flow}(t_{\Delta t}) > I_{LTE,i}$ for all $\Delta t \in TTF_{STE,i''}$ (or $I_{i,flow}(t_{\Delta t}) > I_{con,i}$ for all $\Delta t \in TTF_{LTE,i''}$). These three conditions are shown in Fig. 2 with the double arrows and the large conditional blocks they connect.

The ***surviving high-loading state*** occurs when the cable is operated for a larger than Δt duration at an emergency rating without failing. Two operating conditions can result in this state: (a) when sufficiently large $TTF_{STE,i''}$ or $TTF_{LTE,i''}$ durations are estimated resulting in a no-failure event, and (b) when operation actions interrupt the high-loading operation before it is manifested to a failure; in other words, the current flow, $I_{i,flow}(t_{\Delta t})$, of a high-loaded cable is reduced to its normal-loading state, at any Δt before its projected $TTF_{STE,i''}$ or $TTF_{LTE,i''}$. The condition (b) could be, for example, the result of a $TTF_{STE,i''}$ (or $TTF_{LTE,i''}$) value of 18 hours with demand drop at night terminating the emergency high-loading state in 6 hours. This is not a normal-loading state as it entails a considerable amount of thermal ageing that needs to be estimated and recorded.

Fig. 3 illustrates an example of the 1st SMC-loop transition mapping with three cables that transition between normal-failure (NLF), high-loading failure (HLF) and cascading failure (CF) states. In Fig. 3(a), it can be observed that the HLF is only mapped from the Δt at which the failure of cable *1'* occurred, (continuous line) leading to high-loading operation of the cable *2* (i.e., *2"*) and initiating the $TTF_{LTE,2''}$ calculation, which leads to its HLF transition after a few Δts. The failure of cable *1'* does not transit $I_{3,flow}$ to the high-loading state. Thus, cable *3* remains at normal-loading (i.e., *3'*). However, at the second event, the failure of cable *2"* results in the current of cable *3* $(I_{3,flow})$ to exceed its $I_{STE,3}$ value. This initiates

the $TTF_{STE,3''}$ calculation for the high-loading operation of cable *3* (i.e., *3″*) at the specific Δt leading to its CF as shown in Fig. 3(a) and (b).

The exact current flows of cables in Fig. 3(b) indicate the actual high-loading and transition times. These are segmented to execute the failure occurrences at the beginning of every Δt and the recoveries at the end of every Δt as shown in Fig. 3(c). Hence, the HLF and CF transitions are modelled as they occur at the same time. This procedure captures the maximum unavailability of the cables; however, it does not capture the complete duration of expected elevated temperature operation and the corresponding ageing of the cables.

C. 2nd SMC-Loop Component Life-Cycle Computations

The 2nd SMC-loop captures the entire emergency operation history (EDEL) of every cable *i* at a year Y_L of its life-cycle (Y_{Life}) through the proposed coefficient β_{i,Y_L}. Hence, β is determined by (9) and considers the expected increased risk of failures of every cable *i* exposed to frequent emergency loading, and it can quantify the impact of operating history on cables' life. Assuming that a utility employs a risk-averse operating strategy and hence no emergency loadings, EDEL will be zero making β_{i,Y_L} in (9) zero as discussed before.

$$\begin{aligned}\beta_{i,Y_L} &= \mathbf{a}\cdot D_{LTE,i,(Y_L-1)} + \mathbf{b}\cdot D_{STE,i,(Y_L-1)} \\ &= \mathbf{a}\sum_{Y_L=1}^{Y_{Life}} EDEL_{LTE,i,Y_L} + \mathbf{b}\sum_{Y_L=1}^{Y_{Life}} EDEL_{STE,i,Y_L}\end{aligned} \tag{9}$$

In (9), $D_{LTE,i,(Y_L-1)}$ and $D_{STE,i,(Y_L-1)}$ are the accumulated LTE and STE operating durations, in hours, of every cable *i* occurred before year Y_L of its life. **a**, and **b** are parameters affected by the cable materials, technology and manufacturer, and characterize the cable's degradation severity rate due to operation at LTE and STE loadings, respectively. These parameters can be estimated through experimentation data or empirically based on utility experience. The EDELs for LTE and STE operations are calculated in the 1st SMC-loop and discussed in Section II-E.

D. Cable Thermal Modelling

The component temperature mapping block (in Fig. 1) converts the current flow, $I_{i,flow}(t_{\Delta t})$, for every network cable *i*, at a given Δt, to its operating temperature $\theta_{C,i}(t_{\Delta t})$. Both steady-state, SS-$\theta_{C,i}(t_\theta)$, and transient-state, TS-$\theta_{C,i}(t_\theta)$, temperatures of the conductor are calculated following the process shown in Fig. 4. The steady-state (SS) thermal model calculations use $t_\theta = \infty$, while the transient-state (TS) model considers $t_\theta = \Delta t$.

The input data for these calculations are the cable system data, and the computed cable current flows, $I_{i,flow}(t_{\Delta t})$, at the given Δt. Cable system data include cable design configuration and technology/material properties describing the cable type (e.g., paper or XLPE), cable size, phases (single core or three cores), internal configuration (with or without armour) and the soil material properties (thermal resistivity and volume specific heat). Additional information is related to laying formation, installation depth and soil temperatures. Thus, the cable thermo-electric equivalent (TEE) model can be formulated.

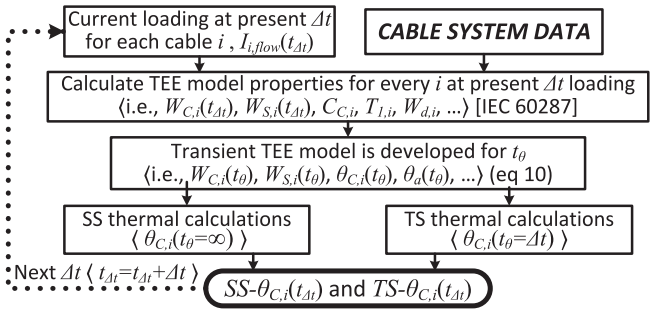

Fig. 4. Cable temperature mapping flowchart at Δt.

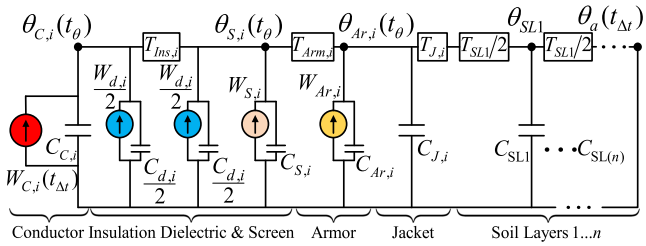

Fig. 5. Time-dependent TEE model considered for single core cables.

TABLE I
CABLE MODELLING—THERMAL MATRIX **M** & LAYER THERMAL PROPERTIES

Calculation of thermal matrix M elements (M_{ij})	
Left-diagonal	$M_{ij} = 1/(C_{SL(n+1-i)} \cdot T'_{(n+1-i)})$, for i=1, 2,⋯, n+m, j=i-1
Right-diagonal	$M_{ij} = 1/(C_{SL(n+1-i)} \cdot T'_{(n-i)})$, for i=1, 2,⋯, n+m, j=i+1
Diagonal	$M_{ii} = -(M_{i(i-1)} + M_{i(i+1)})$, for i=1, 2,⋯, n+m
Calculation of layer k thermal capacitance, $C_{SL(k)}$, and resistance, $T'_{(k)}$	
Layer thermal resistance $T'_{(k)}$	$T'_{(k)}=T_{SL(k)}/2+T_{SL(k+1)}/2$, k = 1, 2,⋯, n-1, n for soil $T'_{(0)}=T_J+T_{SL1}/2$ $T'_{(-1)}=T_{Ar}$ $T'_{(-2)}=T_{Ins}$ } , k = -m, -m+1,⋯,0 for cable
Layer thermal capacitance $C_{SL(k)}$	$C_{SL(k)}$, k = 1, 2,⋯, n-1, n for soil $C_{SL(0)}=C'_J=C_J+C_{Ar}$ $C_{SL(-1)}=C_S+C_d/2$ $C_{SL(-2)}=C'_C=C_C+C_d/2$ } , k = -m, -m+1,⋯,0 for cable
Calculation of external thermal power in layer k	
Layer external thermal power $P_{T\text{-}k}$	$P_{T\text{-}\alpha}=\theta_a(t_{\Delta t})/(C_{SL(n)}\times T'_{(n)})$, $P_{T\text{-}Ar}=W_{Ar}/C_{SL(0)}$, $P_{other}=0$ $P_{T\text{-}S}=(W_S+W_d/2)/C_{SL(-1)}$, $P_{T\text{-}C}=(W_C+W_d/2)/C_{SL(-2)}$

1) Thermo-Electric Equivalent (TEE) Model: The TEE models are implemented based on IEC60287. In the simulation, TEE models consider conductor losses at present Δt, $W_{C,i}(t_{\Delta t})$ (Fig. 5). Thus, time-dependent TEE models are used to calculate the conductor temperature, $\theta_{C,i}(t_\theta)$, using a transient thermal model [10]. The formulation of the transient TEE model of any cable is derived with the matrix equation as in the example of (10), with three conductor and three soil layers

for simplicity, and the generic definitions as in Table I.

$$\begin{bmatrix} \dot{\theta}_{\mathrm{SL3}} \\ \dot{\theta}_{\mathrm{SL2}} \\ \dot{\theta}_{\mathrm{SL1}} \\ \dot{\theta}_{\mathrm{Ar}} \\ \dot{\theta}_{\mathrm{S}} \\ \dot{\theta}_{\mathrm{C}} \end{bmatrix} = \begin{bmatrix} \mathrm{M}_{11} & \mathrm{M}_{12} & 0 & 0 & 0 & 0 \\ \mathrm{M}_{21} & \mathrm{M}_{22} & \mathrm{M}_{23} & 0 & 0 & 0 \\ 0 & \mathrm{M}_{32} & \mathrm{M}_{33} & \mathrm{M}_{34} & 0 & 0 \\ 0 & 0 & \mathrm{M}_{43} & \mathrm{M}_{44} & \mathrm{M}_{45} & 0 \\ 0 & 0 & 0 & \mathrm{M}_{54} & \mathrm{M}_{55} & \mathrm{M}_{56} \\ 0 & 0 & 0 & 0 & \mathrm{M}_{65} & \mathrm{M}_{66} \end{bmatrix} \times \begin{bmatrix} \theta_{\mathrm{SL3}} \\ \theta_{\mathrm{SL2}} \\ \theta_{\mathrm{SL1}} \\ \theta_{\mathrm{Ar}} \\ \theta_{\mathrm{S}} \\ \theta_{\mathrm{C}} \end{bmatrix} + \begin{bmatrix} \mathrm{P}_{\mathrm{T}-\alpha} \\ 0 \\ 0 \\ \mathrm{P}_{\mathrm{T\text{ - }Ar}} \\ \mathrm{P}_{\mathrm{T\text{ - }S}} \\ \mathrm{P}_{\mathrm{T\text{ - }C}} \end{bmatrix} \tag{10}$$

The equations in Table I calculate the cable's TEE model thermal matrix, **M**, for modelling both soil and cable layers. *n* is the soil layer number and *m* is the number of the cable's conductive component layers. The multi-layer soil model based on the exponential discretization approach in [20] is used to formulate each layer's T-equivalent thermal resistance and capacitance.

$C_{\mathrm{SL}(k)}$ and $T'_{(k)}$ indicate thermal capacitance and resistance of the TEE model of layer *k*, $\forall k \in \{-m, -m+1, -m+2, \cdots, n\}$ (Table I). Positive *k* values indicate soil layers, $k = 0$ indicates the cable's jacket layer (e.g., C'_J, T_J), while negative *k* values indicate the layers for the conductive components of the cable model (e.g., armour, sheath and core) with the highest negative value referring to the conductor. $\mathrm{P}_{\mathrm{T}\text{-}k}$ in (10) captures the external thermal power induced in layer *k* of the TEE cable model.

2) Cable Thermal Ageing Modelling: The calculated SS-$\theta_{C,i}(t_{\Delta t})$, and TS-$\theta_{C,i}(t_{\Delta t})$, temperatures at present Δt, feed into the ageing computations performed using the Arrhenius model to calculate the loss-of-life fraction for each cable expected at Δt, $LF_{\theta_{C,i}}(t_{\Delta t})$. This model is described by (11) and considers the insulating material degradation speed, for operation above the ambient reference temperature $\theta_{o,i}$, which is exponentially affected by the material's activation energy, Ea_i. $L_{o,i}$ is the expected life of cable *i* when it operates at $\theta_{o,i}$, and k_B is the Boltzmann's constant (in eV/K). To allow for the comparative ageing evaluation of the different network cables and high-loading events, the equivalent cable ageing (ECA) index is proposed and described by (12). This calculates the cables' equivalent ageing at 90 °C, which is the common maximum continuous temperature used by utilities.

The proposed ECA index is, thus, important for equating all the different high-loading events to a thermal per-unit base value, hence, allowing for their aggregation to formulate the past service experience of the cables but also facilitating the comparison of different cables within the same network.

$$LF_{\theta_{C,i}}(t_{\Delta t}) = \frac{\Delta t}{L_{o,i} e^{-(Ea_i / k_B)(1/\theta_{o,i} - 1/\theta_{C,i}(t_{\Delta t}))}} \tag{11}$$

$$\mathrm{ECA}_{i,\Delta t} = \frac{LF_{\theta_{C,i}(t_{\Delta t})}}{LF_{i,\,90^{\circ}\mathrm{C}}} = \exp\left(\frac{Ea_i}{k_B}\left(\frac{1}{363} - \frac{1}{\theta_{C,i}(t_{\Delta t})}\right)\right) \tag{12}$$

E. Cable and Network Performance Indices

Cable and network performance indices are calculated with the DSMC method. The 1st SMC-loop is the analysis for year *Y*, $\forall Y \in \{1, \cdots, N\}$ for every network cable *i* and the 2nd SMC-loop is the life-cycle analysis in annual steps Y_L, $\forall Y_L \in \{1, \cdots, Y_{Life}\}$. As the life-cycle loop uses the risk coefficient β_{i,Y_L} given by (9), all indices are Y_L-dependent by definition, as shown in (13).

$$INDEX_{i,Y_L} \equiv f(\lambda, U_{i,Y_L}) \equiv f(\alpha, \beta_{i,Y_L}) \tag{13}$$

The cable performance indices are computed with (14)–(19). The ECA is recorded for every cable *i* and Δt within the *Y* period of study (1st SMC-loop in Fig. 1) with EECA being the mean expected ECA of *N* total number of *Y* simulation periods, in the specific year Y_L of cable's life-cycle (Y_{Life}). The EFCF is the expected average number of normal $(NCF_{i,Y})$ and emergency $(ECF_{i,Y})$ cable failures. The EDELs, for both LTE and STE operation, are the mean values for the life-cycle year Y_L; they are computed from the total short $(d_S TE_{i,Y})$ and long $(d_L TE_{i,Y})$ emergency loading durations, for each cable *i* in each year *Y*. The EDEL computes the total duration of emergency loading, while the EFEL captures the mean number of emergency loading events $N_e me_{i,Y}$ for each cable *i* in each year *Y*. The last two indices are very useful in order to obtain the mean expected high-loading duration per emergency event and thus can forecast the expected impact of cable ageing on network considering the operator's emergency actions.

$$EECA_{i,Y_L} = \sum_{Y=1}^{N}\left(\sum_{\Delta t=1}^{Y} ECA_{i,\Delta t}\right) \Big/ N \tag{14}$$

$$EFCF_{i,Y_L} = \sum_{Y=1}^{N}\left(NCF_{i,Y} + ECF_{i,Y}\right) \Big/ N \tag{15}$$

$$EDEL_{LTE,i,Y_L} = \sum_{Y=1}^{N}\left(d\_LTE_{i,Y}\right) \Big/ N \tag{16}$$

$$EDEL_{STE,i,Y_L} = \sum_{Y=1}^{N}\left(d\_STE_{i,Y}\right) \Big/ N \tag{17}$$

$$EDEL_{i,Y_L} = EDEL_{STE,i,Y_L} + EDEL_{LTE,i,Y_L} \tag{18}$$

$$EFEL_{i,Y_L} = \sum_{Y=1}^{N} N\_eme_{i,Y} \Big/ N \tag{19}$$

The network performance indices are computed by (20)–(24), where, the load curtailment duration (LCD_Y), the number of load curtailment events (LCE_Y), and the system energy not supplied ($SysENS_Y$) are recorded for every *Y* (of total *N* times) in the 1st SMC-loop. The EENA and EFNF capture the total (annual) network ageing and network component failures in Y_L. These are very useful indicators for network overall asset management evaluation as they can capture the ageing per failure and hence the network resiliency to failures. In other words, they can assess the network's overall ageing condition and identify the optimal cable replacement strategy based on minimizing the overall network ageing per failure. They can help utilities to optimally prioritize new cable installation in a network with many existing cables of similar age.

EFNF captures the network component failures and is a different index from the EFLC. There might be failures that do not lead to EFLC as the emergency loading can increase network flexibility to "serve the load". Equally, a specific failure in the line can result in more than one load curtailment (indicating a critical failure or a cascading event). These two indices in combination with the EENA can quantify the network resilience to failures. In other words, a large EFNF and a low EFLC with low EENA indicate a resilient network, and vice versa. These indices can, thus, capture the effect of emergency loadings on network resilience and optimize their rating values.

$$EDLC_{Y_L} = \sum_{Y=1}^{N} LCD_Y \Big/ N \tag{20}$$

$$EFLC_{Y_L} = \sum_{Y=1}^{N} LCE_Y \Big/ N \tag{21}$$

$$EENS_{Y_L} = \sum_{Y=1}^{N} SysENS_Y \Big/ N \tag{22}$$

$$EENA_{Y_L} = \sum_{i=1}^{N_C} EECA_{i,Y_L} \tag{23}$$

$$EFNF_{Y_L} = \sum_{i=1}^{N_C} EFCF_{i,Y_L} \tag{24}$$

F. Network Optimization Calculations

The network optimization is implemented using (25) after the initial network component status mapping (Fig. 1) is performed, and including any additional high-loading failures identified at any previous Δt, as expected to occur in the present Δt. The calculations use an AC optimal power flow (ACOPF) to minimize the total generation and load curtailment costs subject to predefined network operational constraints (i.e., generation output capability and speed, G_y, and voltage limits on network buses, V_j) and cable system constraints (i.e., cable maximum flows, $S_{\max,i}$), set in the network and cable data blocks (Fig 1).

$$\mathbf{Min}\left(\sum_{\mathbf{x}}^{\mathbf{N_D}} \left(\mathbf{f_D^x}\left(\mathbf{D^x_{actual}} - \mathbf{D^x_{total}}\right)\right) + \sum_{y}^{N_g}\left(f_P^y\left(p_g^y\right) + f_Q^y\left(q_g^y\right)\right)\right) \tag{25}$$

subject to:

$$-\mathrm{S}_{\max,i} \le \mathrm{S}_i \le \mathrm{S}_{\max,i},\ \mathrm{G}_{\min,y} \le \mathrm{G}_y \le \mathrm{G}_{\max,y},$$

$$V_{\min,j} \le V_j \le V_{max,j}$$

All loads are considered as negative (consuming) generators in order to be dispatched within the ACOPF problem under constrained network conditions. Their cost coefficients are set to have much higher values compared to the most expensive unit in the network. Thus, the optimization re-dispatches first all the actual plant generators, *y*, by considering the sum of their cost functions, f_P^y, f_Q^y, for the real, p_g^y, and reactive, q_g^y, power outputs. Then it re-dispatches the load (negative) generators as a secondary option. The re-dispatching of the load generators reduces the load aiming to minimize the total load curtailment of the constrained network. This is calculated as the difference between the actual supplied load, D^x_{actual}, and the total required load, D^x_{total} in (25). Hence, the interruption costs are also minimized since (25) considers the amount of load curtailment and the damage cost function, f_D^x, at each one of the system load points, *x*, according to [29].

III. Implementation of the Proposed Reliability Evaluation Framework on an UGC Network

The proposed methodology is applied on the IEEE 14-bus network with increased default demand to 1.6 pu. Only cable failures are modelled while all other components are assumed to be 100% reliable with their nominal capacity increased to 2 pu. The IEEE RTS-96 chronological load profiles were adopted to describe the hourly load profile for the test network [13].

A. Selection of Test Cable Properties

The IEEE 14-bus network does not provide thermal limits and circuit design data; therefore, these were retrieved from manufacturers' datasheets [31], [32] with the resulting values for the variables shown in Table II. Four types of single-core unarmoured XLPE cables with copper conductors are used in the study (Table II). The cables are assumed to be in flat lay formation with a conductor separation of 0.1 m and directly buried at 0.8 m and 1.5 m depths for 13.8 kV and 69 kV respectively. Normal, STE and LTE loading capabilities are utilized to provide flexibility at contingencies. Their I_{LTE} and I_{STE} ratings are 1.103 and 1.143 times the maximum normal continuous current, I_{con}, which are the same proportions (i.e., I_{LTE}/I_{con}, and I_{STE}/I_{con}) of the 132 kV cable adopted in RTS-96 [13]. The cables' thermal ratings, also shown in Table II, are calculated at

TABLE II
CABLE ELECTRICAL PROPERTIES MODELED IN IEEE 14-BUS NETWORK

Cables Type	Size mm^2	$R_{90\,^\circ C}$ Ω/km	X Ω/km	B S/km	I_{Con} A [°C]	I_{LTE} A [°C]	I_{STE} A [°C]
A	400	0.060	0.119	6.49×10^{-5}	790 [90°]	871 [111°]	903 [121°]
B	630	0.038	0.109	8.38×10^{-5}	1010 [90°]	1114 [110°]	1154 [119°]
C	400	0.063	0.094	1.41×10^{-4}	845 [90°]	932 [111°]	966 [121°]
D	800	0.035	0.087	1.98×10^{-4}	1200 [90°]	1323 [110°]	1371 [119°]

TABLE III
CABLE RELIABILITY PROPERTIES MODELED IN IEEE 14-BUS NETWORK

Cable No.	From Bus	To Bus	Voltage Level [kV]	Length [miles]	Outage Rate [Occ./yr]	Outage Duration [hr/Occ.]	Cable Type
1	1	2	69	8.47	0.279	24.2	B
2	1	2	69	8.47	0.279	24.2	B
3	1	5	69	15.61	0.323	34.9	A
4	2	3	69	13.84	0.312	32.3	A
5	2	4	69	12.63	0.304	30.4	A
6	2	5	69	12.44	0.303	30.2	A
7	3	4	69	12.49	0.303	30.2	A
8	4	5	69	3.00	0.245	16.0	A
9	6	11	13.8	0.60	0.230	12.4	C
10	6	12	13.8	0.77	0.231	12.7	C
11	6	13	13.8	0.40	0.228	12.1	D
12	9	10	13.8	0.25	0.228	11.9	C
13	9	14	13.8	0.81	0.231	12.7	C
14	10	11	13.8	0.57	0.230	12.4	C
15	12	13	13.8	0.81	0.231	12.7	C
16	13	14	13.8	1.05	0.233	13.1	C

15 °C soil temperature, 0.9 km/W soil thermal resistivity, and 1.9×10^6 J/m^{3}K volume specific heat, which are the default values in ENA P17 [1].

The length of every circuit, ℓ_i, (in miles) is required to determine the cable failure and repair rates defined by (26) from [33] and (27). The latter, is derived by the authors in order to fit the cable data provided in [33]. The IEEE 14-bus system [34] does not provide the lengths. These are derived using the original impedance data and the 0.7 Ω/mile factor in [35]. The produced length and reliability data along with the cable types used in this modified 14-bus cable network are shown in Table III.

$$\lambda_{N,i} = 0.0062 \times \ell_i + 0.226 \ (\text{occ.} / \text{yr}) \tag{26}$$

$$1/\mu_{N,i} = 1.5 \times \ell_i + 11.5 \ (\text{hr} / \text{occ.}) \tag{27}$$

Finally, a time-varying soil temperature measurement profile is used for this analysis obtained from ERA-interim dataset for the year 2015 provided by [36]. An Arrhenius model parameter (Ea_i/k_B) value of 12430 K is used in this example to determine that the network's cables are XLPE technology [11].

B. Modelled Scenarios

The proposed methodology is applied to the modified 14-bus network to study the flexibility and operation risk under the high-loading emergency ratings (ERs) scenarios of Table IV. These scenarios are compared against the base-case scenario (BC) to quantify any improvements or limitations from increased cable utilization during emergencies. Sc-1 implements both LTE and STE ERs without including any additional risk at emergency loading (i.e., $\alpha = \beta = 0$). Sc-2 captures three different levels of increased risk of high-loading failures which reflect constraint cable designs with joints that experience unfavorable laying conditions (i.e., $\alpha \neq 0$, $\beta = 0$). Sc-3 considers equivalent pre-set values of increased risk at emergency operation for both the cable design risk of failure and operator's risk acceptability. Finally, Sc-4 fully utilizes the 2nd SMC-loop to capture the expected ageing history of the cables due to the operator's decision to deploy emergency loadings. α in Sc-4 is constant as the cable design and laying conditions are assumed independent of cables' age.

TABLE IV
MODELLING SCENARIOS OF EMERGENCY UGC RISK OF FAILURE

Scenarios		Model Variables	Description of risk
Base Case		No Emergency Ratings (ERs) Employed	
high-load ERs failures	Sc-1	$\alpha = 0\ \beta = 0$	ERs + no increased risk
	Sc-2	$\alpha = 10, 20, 30\ \beta = 0$	ERs + unfavorable cable laying risk
	Sc-3	$\alpha = \beta = 10, 20, 30$	Sc-2 + fixed annual lifecycle ageing
	Sc-4	$\alpha = 10, \beta \equiv (9)$ & $\mathbf{a} = 0.05$, $\mathbf{b} = 0.2$	Sc-2 + operation-based lifecycle ageing (different ageing in cables)

TABLE V
SUMMARY OF NETWORK PERFORMANCE INDICES

	Scenario coefficients	EENS MWh/yr	EFLC Occ./yr	EDLC hr/yr	EFNF Occ./yr	EIC M $	$EENA_{TS}$ hr/yr	$EENA_{SS}$ hr/yr
BC	No ER	73.34	2.89	15.18	20.88	1.96	161.97	412.40
Sc-1	$\alpha = \beta = 0$	30.15	1.12	6.07	20.96	0.77	164.47	488.94
Sc-2	$\alpha = 10$	31.16	1.17	6.32	21.15	0.80	164.72	495.32
	$\alpha = 20$	36.47	1.33	7.36	21.67	0.94	165.37	511.18
	$\alpha = 30$	57.99	1.87	10.95	22.82	1.54	167.03	550.23
Sc-3	$\alpha = \beta = 10$	37.48	1.36	7.51	21.75	0.98	165.46	512.42
	$\alpha = \beta = 20$	110.75	3.10	19.34	25.37	3.01	170.46	640.73
	$\alpha = \beta = 30$	429.37	6.67	47.61	30.34	11.92	178.22	824.77

IV. RESULTS & DISCUSSION

A. Impact of Cables' High-Loading Risk on Network Flexibility

The benefits of emergency ratings (ERs) implementation are evident when comparing the outputs of scenarios Sc-1 to Sc-3 with the base-case (BC) scenario in Table V. Sc-1 improves network performance the most due to zero risk related to ERs utilization. The frequencies of network failures (EFNF) for BC and Sc-1 are virtually identical as there are no ERs failures. The comparison of these two scenarios indicates the maximum (ideal) flexibility that could be extracted from the ERs

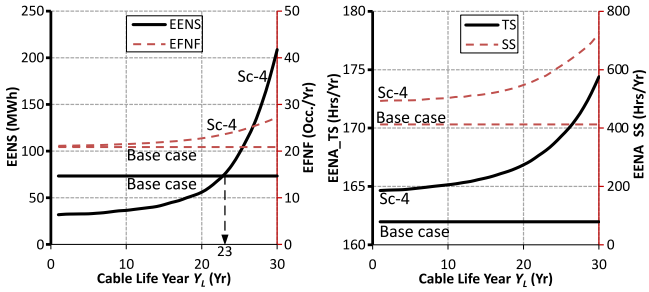

Fig. 6. Comparison of Sc-4 with base-case for EENS, EFNF, and EENA for the complete 30 year of cable's design life.

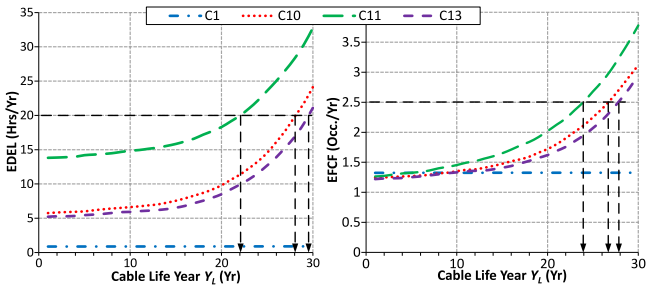

Fig. 7. EDEL and EFCF outputs of critical cables under Sc-4 for the complete 30 year of cable's design life.

deployment on this network. Once the risks of cable design (α) and operator's cable ageing acceptability (β) are considered, then the benefit from the ERs in network performance is reduced. ERs generate additional failures that mainly occur on frequently heavily loaded cables increasing EFNF of Sc-2 and Sc-3 (Table V). Yet, the network still performs better, with less EENS and EIC, due to added flexibility from ERs.

ERs appear to worsen network performance only when high values for α and β are considered (i.e., Sc-3, $\alpha = \beta \geq 20$). The high α and β values could describe the case of applying ERs on an old and poorly maintained cable. In this case, the additional failures overweight the ERs' benefit on flexibility leading to higher EIC values when compared to BC. The comparison of Sc-2 and Sc-3 denotes that the ageing acceptability risk index β has a more notable effect on the ERs failures compared to the cable design risk index α. These results suggest that accelerated cable ageing and insulation degradation, caused by the emergency operation, have a greater impact when they affect the cable's failure rate than when they affect only cables' expected life (determined by the cable design and its laying conditions). Thus, the inclusion of α and β within the methodology provides a realistic modelling of risk from their emergency loading indicating that ER can increase network flexibility when they are not frequently utilized, while an overutilization would decrease the network resilience to contingencies.

Finally, the EENA values from SS and TS thermal models indicate a largely inflated estimate of SS method under both normal and emergency loadings, which suggests that the impact of cable thermal inertia cannot be ignored if utilities want to achieve maximum benefits from their assets and ER implementation. The EENA_{TS} varies insignificantly when ERs are implemented, which indicates that ERs do not affect the cable ageing as much as it is expected with SS calculations.

B. Cable Life-Cycle Analysis

The 2nd SMC-loop is employed in Sc-4 with a 30-year cable design life. The recorded indices change annually, as the 'year in service' increases, following the trends shown in Figs. 6 and 7. On the contrary, the ageing in BC (existing modelling practices) is unaffected by operation history and thus it results in constant performance throughout the cables' life (Figs. 6 and 7).

Sc-4 initially results in better network reliability than the BC due to the increased network flexibility provided by the ERs (Fig. 6). But as the 'year in service' increases and the cumulative effect of emergency operation history builds up, the EENS for Sc-4 further increases and reaches the same value as the BC in year 23. From this year onwards the increased ageing of the cables reduces network's performance (in Sc-4). It should be noted that an aged cable cannot maintain the same reliability as a new one and the BC scenario with a constant failure rate and no ageing impact is unrealistic, and thus does not help the improvement of current planning and operating practices.

In Fig. 6 (right) when the SS thermal model is used, EENA is significantly over-estimated particularly when the cables' 'year in service' increases; this model can lead to 400% more ageing than the actual captured with the TS method. Consequently, the SS thermal model could mislead cable condition assessments when those are based on service history.

The study of individual cable performance in the 14-Bus network identified C10, C11 and C13 as 'critical' cables, encountering ERs much more frequently than the 'low loaded' C1 and the rest of the cables. In Fig. 7 the cables' performance is captured through the EDEL and EFCF for their entire cable life operation. The EDEL is higher for the critical cables from the first year of their operation where the EFCF is almost identical (similar λ in year 1). Hence, EDEL helps to prioritize the network cables based on their risk of failure and accounting for both network topology and individual cable's operational regime (i.e., operator's preferences on thermal loadings). The results shown in Fig. 7 help distinguish C11 as the most critical cable in the network, while C10 and C13 are equally but less critical than the C11. On the contrary, C1 appears to be unaffected from the emergency events with negligible thermal ageing effects.

By setting cable actual performance as a replacement criterion, instead of 'years in service', a projection of C11 replacement on year 22 or 24 is estimated based on the EDEL or EFCF indices respectively (Fig. 7). More importantly, all projections of cables' "useful" life vary based on these new performance indicators. In fact, the EDEL and EFCF estimate the expected replacement time for every cable in the network based on their operation regimes and overall network performance. With the proposed indices operators can be better informed about the condition of their cables. They can also predict future expected ageing based on their present planning and loading decisions and reconsider asset management strategies accordingly.

Operators can correlate these network-based metrics with condition monitoring data to strengthen the robustness of their current cable replacement and maintenance strategies. They can also identify which cables are under-utilized and implement different operating strategies when early replacement is inevitable due to adequacy constraints. From the presented example case study, it can be seen that ECA, calculated by (12), can provide a comparative ageing prediction of individual cables within a network and evaluate overall network resiliency to emergency events via the EENA index. Utilities can therefore cluster the cables considering their high-loading risks into three main groups:

1) *Accelerated ageing cables*: Cables experiencing frequent overloading with a potential effect on their expected design life (e.g., C11). The operator is advised to schedule an outage and perform a comprehensive inspection.
2) *Infrequent high-loaded cables*: Cables experiencing elevated temperature conditions and requiring inspection, monitoring and maintenance (e.g., C10, C13). Future plant outages for measurements might be needed.
3) *Under-utilized cables*: Cable failures would be expected mainly due to exogenous factors and no immediate inspection is needed (e.g., C1 and all remaining network cables).

V. Conclusion

Power networks' current challenge to expand efficiently and increase resiliency to uncertainties can be resolved by implementing flexible operating regimes during emergency conditions. Existing network studies and methodologies fail to simultaneously consider the flexibility of these regimes and their associated thermal ageing risk. The proposed methodology addresses this gap by integrating a detailed thermal and ageing modelling of cable systems within a network reliability analysis. This integration is achieved by using a double sequential Monte Carlo loop, three additional Markov states to describe the cable's emergency operation along with their corresponding transition equations (based on the proposed α and β coefficients), as well as the equivalent cable ageing (ECA) to formulate a common thermal ageing per-unit base for the different emergency events. Thus, the proposed framework can help quantify the impact of increasing risk of failures on network performance, when cables approach their end of life.

The proposed approach significantly improves existing practices, in evaluating network resilience and operator flexibility, by introducing the cable design risk coefficient, α, to relate component condition (health indices) and design, and the operator's ageing risk acceptability coefficient, β, to define the risk-averseness of a utility on 'burning an asset'.

The 14-bus network study indicated three clusters of cables based on their high-loading risks, with the critical ones being objectively identified using the proposed EDEL and EFCF indices.

One limitation of the current work is the lack of utility recorded data to formulate the α and β values. To develop realistic α and β values that fit specific utility networks, cable types and manufacturers, a correlation between the outputs produced by this methodology against experimentally derived data, condition management (health indices) records and utility experience is needed. Coupling this methodology with forecasted demand trends and technology implementation is an additional advancement for improving network reliability and utilization.

References

[1] "Current Rating Guide for Distribution Cables," *ENA Engineering Recomendation P17*, 2004.

[2] "Current rating guide for high voltage overhead lines operating in the UK distribution system," *ENA Engineering Recomendation P27*, 1986.

[3] C. F. Price and R. R. Gibbon, "Statistical approach to thermal rating of overhead lines for power transmission and distribution," *IEE Proc. C—Gener., Transmiss. Distrib.*, vol. 130, no. 5, pp. 245–256, 1983.

[4] Cigre – International Council on Large Electric Systems – Working Group B2.36, "Guide for application of direct real-time monitoring systems—Brochure no. 498," Cigre, Jun. 2012.

[5] K. Kopsidas, A. Kapetanaki, and V. Levi, "Optimal demand response scheduling with real time thermal ratings of overhead lines for improved network reliability," *IEEE Trans. Smart Grid*, vol. PP, no. 99, pp. 1–1, 2016.

[6] J. Yang, X. Bai, D. Strickland, L. Jenkins, and A. M. Cross, "Dynamic network rating for low carbon distribution network Operation—A U.K. application," *IEEE Trans. Smart Grid*, vol. 6, no. 2, pp. 988–998, Mar. 2015.

[7] L. Shuran and K. Kopsidas, "Reliability evaluation of distribution networks incorporating cable electro-thermal properties," in *Proc. 19th Power Syst. Comput. Conf.*, 2016, pp. 1–7.

[8] K. Kopsidas, C. Tumelo-Chakonta, and C. Cruzat, "Power network reliability evaluation framework considering OHL electro-thermal design," *IEEE Trans. Power Syst.*, vol. 31, no. 3, pp. 2463–2471, May 2016.

[9] A. H. Kidder, "Notes on emergency ratings," *Electr. Eng.*, vol. 58, no. 11, pp. 599–610, 1939.

[10] R. Olsen, J. Holboell, and U. S. Gudmundsdóttir, "Electrothermal coordination in cable based transmission grids," *IEEE Trans. Power Syst.*, vol. 28, no. 4, pp. 4867–4874, Nov. 2013.

[11] G. Mazzanti, "Analysis of the combined effects of load cycling, thermal transients, and electrothermal stress on life expectancy of high-voltage AC cables," *IEEE Trans. Power Del.*, vol. 22, no. 4, pp. 2000–2009, Oct. 2007.

[12] *IEEE Recommended Practice for Protection and Coordination of Industrial and Commercial Power Systems (IEEE Buff Book)*, *IEEE Std 242-2001*, 2001, pp. 1–710.

[13] C. Grigg *et al.*, "The IEEE RTS-1996. A report prepared by the reliability test system task force of the application of probability methods subcommittee," *IEEE Trans. Power Syst.*, vol. 14, no. 3, pp. 1010–1020, Aug. 1999.

[14] ISO New York Emergency Operations Manual. [Online]. Available: http://www.nyiso.com/public/webdocs/markets_operations/documents/Manuals_and_Guides/Manuals/Operations/em_op_mnl.pdf. Accessed: Apr. 2016.

[15] ISO New England Operating Procedure No. 19 – Transmission Operations. [Online]. Available: http://www.iso-ne.com/static-assets/documents/rules_proceds/operating/isone/op19/op19_rto_final.pdf. Accessed: Apr. 2016.

[16] PJM Interconnection. PJM Manual 03: Transmission Operations. [Online]. Available: http://www.pjm.com/~/media/documents/manuals/m03.ashx. Accessed: Feb. 2016.

[17] S. H. Huang, W. J. Lee, and M. T. Kuo, "An online dynamic cable rating system for an industrial power plant in the restructured electric market," *IEEE Trans. Ind. Appl.*, vol. 43, no. 6, pp. 1449–1458, Nov./Dec. 2007.

[18] A. Safdarian, M. Z. Degefa, M. Fotuhi-Firuzabad, and M. Lehtonen, "Benefits of real-time monitoring to distribution systems: Dynamic thermal rating," *IEEE Trans. Smart Grid*, vol. 6, no. 4, pp. 2023–2031, Jul. 2015.

[19] Y. C. Liang and Y. M. Li, "On-line dynamic cable rating for underground cables based on DTS and FEM," *WSEAS Trans. Circuits Syst.*, vol. 7, no. 4, pp. 229–238, 2008.

[20] D. J. Swaffield, P. L. Lewin, and S. J. Sutton, "Methods for rating directly buried high voltage cable circuits," *IET Gener., Transmiss. Distrib.*, vol. 2, pp. 393–401, 2008.

[21] M. Diaz-Aguil, F. D. Le, S. Jazebi, and M. Terracciano, "Ladder-type soil model for dynamic thermal rating of underground power cables," *IEEE Power Energy Technol. Syst. J.*, vol. 1, pp. 21–30, 2014.

[22] R. S. Olsen, J. Holboll, and U. S. Gudmundsdottir, "Dynamic temperature estimation and real time emergency rating of transmission cables," in *Proc. 2012 IEEE Power Energy Soc. General Meeting*, 2012, pp. 1–8.
[23] Z. Xiang and E. Gockenbach, "Assessment of the actual condition of the electrical components in medium-voltage networks," *IEEE Trans. Rel.*, vol. 55, no. 2, pp. 361–368, Jun. 2006.
[24] M. Buhari, K. Kopsidas, C. Tumelo-Chakonta, and A. Kapetanaki, "Risk assessment of smart energy transfer in distribution networks," in *Proc. Innovative Smart Grid Technol. Conf. Eur.*, Istanbul, Turkey, 2014, pp. 1–6.
[25] M. Stotzel, M. Zdrallek, and W. H. Wellssow, "Reliability calculation of MV-distribution networks with regard to ageing in XLPE-insulated cables," *IEE Proc.—Gener., Transmiss. Distrib.*, vol. 148, no. 6, pp. 597–602, 2001.
[26] M. Buhari, V. Levi, and S. K. E. Awadallah, "Modelling of ageing distribution cable for replacement planning," *IEEE Trans. Power Syst.*, vol. 31, no. 5, pp. 3996–4004, Sep. 2016.
[27] M. Kellow and H. St-Onge, "Thermo-mechanical failure of distribution cables subjected to emergency loading," *IEEE Power Eng. Rev.*, vol. PER-2, no. 7, pp. 29–30, Jul. 1982.
[28] R. Billinton, M. Fotuhi-Firuzabad, and L. Bertling, "Bibliography on the application of probability methods in power system reliability evaluation 1996-1999," *IEEE Power Eng. Rev.*, vol. 21, no. 8, pp. 56–56, Aug. 2001.
[29] R. Billinton and W. Li, *Reliability Assessment of Electrical Power Systems Using Monte Carlo Methods*. London, U.K.: Springer, 1994.
[30] M. Schilling, R. Billinton, and M. Groetaers dos Santos, "Bibliography on power systems probabilistic security analysis 1968–2008," *Int. J. Emerg. Electr. Power Syst.*, vol. 10, no. 3, pp. 1–48, 2009.
[31] Oman Cables. Medium Voltage Cables Brochure. [Online]. Available: http://omancables.com/wp-content/uploads/2017/01/Medium-Voltage-MZ.pdf. Accessed: Sep. 2016.
[32] Demirer Kablo. High and Extra High Voltage Cable System. [Online]. Available: http://www.demirerkablo.com/media/33103/catalogue.pdf. Accessed: Sep. 2016.
[33] P. M. Subcommittee, "IEEE reliability test system," *IEEE Trans. Power App. Syst.*, vol. PAS-98, no. 6, pp. 2047–2054, Nov. 1979.
[34] R. Christie, IEEE 14-bus Power Systems Test Case. [Online]. Available: http://www.ee.washington.edu/research/pstca/pf14/pg_tca14bus.htm. Accessed: Mar. 2016.
[35] L. L. Grigsby, *Power Systems*, 3rd ed. Boca Raton, FL, USA: CRC Press, 2016.
[36] European Centre for Medium-Range Weather Forecasts (ECMWF). ERA Interim dataset: soil temperature. [Online]. Available: http://apps.ecmwf.int/datasets/data/interim-full-daily. Accessed: 2015.

Konstantinos Kopsidas (M'06–SM'17) is a Lecturer of electrical power engineering and the Director of the M.Sc. in electrical power systems engineering in the School of Electrical and Electronic Engineering, University of Manchester, Manchester, U.K. His research is related to component design aspects and network operation strategies that can improve the resilience and flexibility of electrical power networks. He is expert in the area of overhead lines and underground cables design modelling and reliability/security assessments. He has published more than 50 research papers and reports and has been delivering CPD courses related to OHL in industry and academia.

He is/has been actively involved with a number of EPSRC, EU, and industrial projects. He is convener of a CIGRE WG C4.25, member of the IEEE Grid Code Task Force, consultant for several national and international activities (UKPN, Mott Macdonald, Balfour Beatty) and a member of advisory boards of EU projects (Grid4EU), Quality assurance organisations (H.Q.A.A.A.) and industry (ECOFYS). He is a member of IET.

Shuran Liu (S'15) received the B.Eng. degree in electrical engineering from Hohai University, Nanjing, China, and the University of Strathclyde, Glasgow, U.K., in 2014. He is currently working toward the Ph.D. degree in the Electrical Energy and Power Systems group, University of Manchester, Manchester, U.K. His research interests reside within the broader topics of power system operation, reliability and asset management, with a current emphasis on reliability evaluation of smart grid technologies and renewable energy integration, thermal rating and ageing of power cables and overhead lines.